

pubs.acs.org/acsaenm

Rapid Capture of Per- and Polyfluoroalkyl Substances Using a Self-Assembling Zirconium-Based Metal-Organic Cage

Dino Camdzic, Heshali K. Welgama, Matthew R. Crawley, Anish Avasthi, Timothy R. Cook,* and Diana S. Aga*



ACCESS I

ACS APPLIED

Cite This: ACS Appl. Eng. Mater. 2024, 2, 87–95

Metrics & More



Article Recommendations

N-MeFOSAA **PFOA PFOS** N-MeFOSAA

ABSTRACT: Legacy and emerging per- and polyfluoroalkyl substances (PFAS) are widely detected in environmental and human samples because of their widespread use and resistance to degradation. Due to the increasing concern on health impacts of PFAS resulting from exposure to contaminated water, the development of novel materials to capture and remove PFAS from the environment is needed. Here, we present a self-assembling, fluorinated, zirconium-based metal-organic cage (F-ZrMOC) capable of capturing 37 different PFAS species, at an average of 82% removal from a solution that contains 400 ng/mL of each individual PFAS. The F-ZrMOC captured different classes of PFAS within 30 s, including perfluoroalkyl carboxylates, sulfonates, sulfonamides, ethoxylates, and fluorotelomer carboxylates/sulfonates/alcohols from water during in-vial, static, and flow through exposures (in which the F-ZrMOC is used as a solid phase extraction sorbent). Removal efficiency is higher for PFAS with chain lengths of seven carbons or higher; the presence of complex matrices such as untreated wastewater and groundwater samples did not significantly reduce the removal efficiencies for PFAS. The F-ZrMOC was characterized using ¹H and ¹⁹F nuclear magnetic resonance (NMR) spectroscopy, and the stoichiometry of the synthesized cage was confirmed using Fourier transform-ion cyclotron resonance mass spectrometry. The surface area and pore size of F-ZrMOC were further determined by N₂ and CO₂ sorption measurements. ¹⁹F-NMR spectroscopy revealed that solvent plays an important role in the capture of PFAS; once the cages are in contact with methanol solution, captured PFAS are released.

KEYWORDS: PFAS, metal—organic cage, remediation, environment, wastewater, LC-MS/MS

1. INTRODUCTION

Per- and polyfluoroalkyl substances (PFAS) have been used since the 1940s in a wide range of applications, including nonstick coatings, food packaging materials, medical plastics, mining operations, and aqueous film forming foams (AFFF).¹ The PFAS class of chemicals contains >12,000 compounds according to the EPA CompTox PFAS Master List.² Their widespread use and persistence have led to the detection of PFAS in human serum, animal tissues, soil, and water samples across the globe.³⁻⁶ It has been estimated that 98% of people in the United States (US) have detectable levels of PFAS in their blood. Due to the known toxicity of legacy PFAS, there has been a shift to manufacture and use alternative shorter chain and ether-containing PFAS (also known as emerging

PFAS) to comply with regulations to phase out legacy PFAS.^{8,9} However, the partial degradation of legacy and emerging PFAS leads to shorter chain degradation products that remain persistent in the environment. 10,11

The PFAS degradation products present substantial analytical challenges related to unknown detection and identification in the absence of reference standards. 12 Further,

Received: September 27, 2023 Revised: November 28, 2023 Accepted: November 29, 2023 Published: December 18, 2023





Supporting Information

short-chain PFAS and degradation products are often lost during solid-phase extraction (SPE) and escape detection in liquid chromatography with mass spectrometry (LC-MS) because of their limited sorption capacity and poor retention in reversed phase columns. ^{13,14} Legacy and emerging PFAS, and their degradation products are not effectively removed in conventional wastewater treatment processes, and end up being released into the environment through discharge of treated wastewater into surface water and land application of biosolids. ^{15–18} The widespread occurrence of both legacy and emerging PFAS, along with their documented deleterious effects in humans and wildlife, highlights the critical need to develop rapid and robust methods for capturing a broad class of PFAS to mitigate their release into the environment.

Currently, several materials exist for the capture of PFAS from water, including activated carbon, ¹⁹ functionalized hollow nanoparticles, ²⁰ and metal—organic frameworks (MOFs). ^{21,22} Activated carbon (AC) is used extensively to remove PFAS from drinking water, with varying results. Removal of longer chains occurs with 60%—70% efficacy, while that of shorter chains is much less. ¹⁹ This pattern is further shown in work by He et al. ²³ where emerging and shorter chain PFAS are not well retained by AC, with removal ranging from 1% to 23%. ²³ Even though the capture of long-chain PFAS exceeds 90%, a 40 min equilibration time was required. Although relatively inexpensive to regenerate (\$0.65/lb of AC²⁴) and widely available, AC is not a viable long-term solution due to its low specificity, especially as emerging PFAS become more prevalent.

As an alternative to AC, hollow polystyrene nanoparticles have been synthesized and functionalized with $-\mathrm{CF_3}$ groups to enhance PFAS capture. PFAS removal exceeded 90% for 20 PFAS with chain lengths of 5–14 carbons across critical carboxylic, sulfonic, and ether classes and >80% removal for the perfluorobutanoic acid (PFBA) and perfluorobutane sulfonic acid (PFBS). In samples of Suwannee River natural organic matter with a dissolved organic carbon concentration of 82.7 mg/L, PFAS removal rates lowered but still remained capable of >80% removal consistently. However, to achieve the reported removal, particles functionalized with cystamine were used to adsorb 22 PFAS, each at a concentration of 1 ng/mL for 15 min, requiring equilibration in samples which is not ideal for full-scale environmental remediation. On the sample of th

Previous work by Li et al. reported the synthesis of a zirconium based MOF that has ability to capture PFAS. 21 The three-dimensional nature of the MOF generated large surface areas with meso- and micropores for PFAS adsorption, resulting in more than 90% removal for seven PFAS from water, including the short-chain PFBA. The described MOF is regenerable via HCl/methanol wash and can be reused up to five times for PFAS removal without loss in efficiency. 21,22 Importantly, synthesis can be achieved in one step with care to avoid insoluble byproducts.²⁵ When applied to environmental samples, removal remained efficient for PFAS longer than seven carbons in length, but the removal rates decreased for short-chain PFAS, indicating that matrix inhibited sorption onto the MOF. Specifically, in one sample with very high conductivity (26,300 μ S/cm), removal decreased 2- or 3-fold compared to other samples with lower conductivities (22-310 μ S/cm), suggesting that high concentrations of salt affect MOF-PFAS interactions.²¹ When tested with an expanded set of 28 PFAS and 11 groundwater samples, similar patterns were observed. Longer chain PFAS (C₇-C₁₀) removals were

between 60% and 80%, and shorter chain PFAS (C_4-C_6) exhibited removals of only ~30% overall. The work concluded that the MOF was inhibited by competitive sorption of matrix components, limiting the applicability of the MOF due to its lack of selectivity. Sini et al. investigated the capture of perfluorooctanoic acid (PFOA) and perfluorooctane sulfonic acid (PFOS) using UIO-66 and a perfluorinated UIO-66 and reported a higher uptake by the perfluorinated analogue due to fluorine–fluorine interactions. ²⁶

Interest in metal-organic cages (MOCs) is growing for various applications including separations, 27,28 catalysis, 29,30 and pollutant removal, 31,32 due to their structural tunability, intrinsic porosity, and solution processability. Whereas MOFs are coordination polymer networks that can extend infinitely, MOCs self-assemble to give discrete molecular structures, forming single thermodynamically favored products.^{33,34} This self-assembly is due to interactions between Lewis basic donor ligands and metal-ion acceptors. Although MOFs contain more pores than MOCs due their network structures, the latter can bypass the issue of pore accessibility and substrate diffusion of the former.³⁵ We have previously reported an Fe-based cage that can interact with PFAS and demonstrated removal from water across a variety of species with varying efficacy.³⁶ The Fe-based cage showed substantial interactions with long chain (>C₆) carboxylic and sulfonic PFAS, with 45%-99% and 80%-99% removal, respectively. However, these Fe-based MOCs did not capture shorter chain PFAS of both the carboxylic and sulfonic classes (C_4-C_6) . Analysis by ¹⁹Fnuclear magnetic resonance spectroscopy (19F-NMR) revealed that PFAS bind to the outside surface of the Fe cage, where grooves and clefts likely promote noncovalent interactions. Although the internal cavities of these cages were not large enough to host an entire PFAS molecule, partial penetration into the hydrophobic core may also promote PFAS-cage interactions.3

In this present study, we synthesized a tetrahedral zirconium-based MOC (F-ZrMOC) with four (Cp₃Zr₃µ₃- $O(\mu_2\text{-OH})_3$ (Cp = η^5 -C₅H₅) nodes and six 2,3,5,6-tetrafluoro-1,4-benzenedicarboxylate linkers as edges and evaluated its ability to remove 40 commonly detected PFAS, with diverse functional groups and varying chain lengths. A Zr-based cage was selected due to the stability of this class of MOCs in the presence of water.³⁷ We hypothesized that the C-F groups in the cage linker could promote improved MOC interactions with PFAS molecules. We further hypothesized that the same C-F groups would increase hydrophobicity, preventing the cage from dissolving in the aqueous solution containing PFAS, which enables collection of the cage for analysis of sorption post-PFAS capture experiments. 38 To demonstrate the potential of MOCs for PFAS capture from aqueous solutions, ZrMOCs with four different linkers were evaluated using different quantities to determine optimum equilibration times in flow-through conditions, and treated wastewater effluent was used to investigate effect of environmental matrices in the MOC-PFAS interactions.

2. MATERIALS AND METHODS

2.1. Materials and Methods

Solid PFAS standards were purchased from Acros Organics (Geel, Belgium), Alfa Aesar (Haverhill, MA), Apollo Scientific (Stockport, United Kingdom), Fisher Scientific (Waltham, MA), Matrix Scientific (Elgin, SC), Santa Cruz Biotechnologies (Dallas, Texas), Sigma-Aldrich (St. Louis, MO), Synquest (Atlanta, GA), TCI (Tokyo,

Figure 1. Schematic representation of the fluorinated MOC synthesis. The nodes of the cage $(Cp_3Zr_3\mu_3-O(\mu_2-OH)_3)^{4+}$ are linked by tetrafluoro-1,4-dicarboxylate bridging ligands, resulting in a cationic tetrahedral cage charged balanced by four chlorides.

Japan), and Toronto Research Chemicals (Toronto, Ontario). A mixture of 19 isotopically labeled PFAS (MPFAC-24ES) was purchased from Wellington Laboratories (Overland Park, KS). Zirconocene dichloride was purchased from Strem Chemicals, and tetrafluoroterephthalic acid was purchased from TCI America. Type I water (18.2 $M\Omega\cdot\text{cm}^2$ resistivity) was acquired via a Barnstead Nanopure Diamond filtration system.

PFAS were separated and quantified using a Restek Raptor C_{18} 2.7 μ m, 100 mm \times 3 mm (Bellefonte, PA) on an Agilent 1200 liquid chromatography system (Santa Clara, CA) and Thermo TSQ Quantum Ultra triple quadrupole mass spectrometer (LC-MS/MS) (Waltham, MA) operated under selected reaction monitoring mode (Table S1). Aqueous and organic mobile phases consisted of 5 mM ammonium acetate in water (pH 3.8) and 1:1 acetonitrile:methanol, respectively, at a flow rate of 0.370 mL/min with gradient conditions shown in Figure S9. Results were processed using Thermo Xcalibur 3.2 software. Flow-through tests to establish the applicability of the F-ZrMOC as a passive filter for PFAS were performed using a Mandel Scientific TXA-04 AOX adsorption system (Ontario, Canada).

¹H and ¹⁹F NMR spectra for F-ZrMOC pre- and post-treatment were acquired on a Bruker AVANCE NEO 400 (9.4 T, operating at 400 MHz (¹H) and 376.5 MHz (¹⁹F)) or NEO 500 (11.75 T, operating at 500 MHz (1H) and 470.4 MHz (19F)) NMR spectrometers (Billerica, MA). Chemical shifts (δ) are reported in parts per million (ppm) relative to the residual proton solvent peaks for ¹H NMR or the trifluoroacetic acid peak for ¹⁹F NMR. ¹⁹F DOSY NMR spectra were acquired at 470.4 MHz using a dstebpgp3s pulse sequence. The length of the diffusion gradient (δ) was set to 2 ms, and the diffusion time (Δ) was set to 46.7 ms. The gradient strength (gpz6) varied from 5% to 95% across 16 steps (TD1). At each step, 16 transients (NS) were acquired. Data were processed in Bruker TopSpin, and diffusion analysis was performed using the Bruker Dynamics Center software suite. High resolution mass spectra to confirm m/z of F-ZrMOC were acquired on a Bruker Solarix 12T ESI-FT-ICR (Billerica, MA). The $\,\mathrm{N}_2$ and $\,\mathrm{CO}_2$ sorption isotherms were collected for the F-ZrMOC at 77 and 273 K, respectively, to calculate the surface area and the pore size of the cage, using a Micromeritics 3Flex Adsorption Analyzer. Ultrahigh-purity gases (99.999%) were used for analysis (N2 and CO2) and free space measurements (He). Prior to measurements, all F-ZrMOC samples were activated by evacuating in a vacuum oven at room temperature, until no change in mass was observed (24-48 h), and then transferred to a preweighed sample tube and degassed further in the Micromeritics VacPrep sample preparation system at 30 °C until no change in mass was observed (~24 h). The sample tube with the sample was weighed following the degassing as well as after the measurement. A powder X-ray diffraction (PXRD) pattern was collected from a Rigaku Ultima IV X-ray diffractometer (Tokyo, Japan) equipped with a Cu K α source and operated at 1.76 kW power (40 kV, 44 mA). The diffraction pattern was measured over a 2θ range of 5°-80° at a scan rate of 2°/min. Scanning electron microscopy (SEM) images were acquired using a Carl Zeiss AURIGA electron microscope. The cage sample was gold coated to improve its conductivity before imaging using a sputter coater system (SPI Module) for 30 s.

Fourier transform infrared (FTIR) spectra were acquired from a PerkinElmer 1760 FTIR spectrometer with an attenuated total reflectance (ATR). Powdered samples were used for the measurements. ATR and baseline corrections were performed for all measurements. Spectra were normalized by using the Spectrum software available with the PerkinElmer 1760 instrument.

2.2. Synthesis of Metal-Organic Cage

The MOC synthesis was adapted from the literature.³⁹ Briefly, zirconocene dichloride (bis(cyclopentadienyl)zirconium dichloride) (350.77 mg, 1.2000 mmol) and tetrafluoroterephthalic acid (142.85 mg, 0.6000 mmol) were added into a 50 mL round-bottomed flask and dissolved in 20 mL of dimethylformamide (DMF). Deionized water (0.5 mL) was added into this reaction mixture, and the solution was heated at 65 °C for 20 h (Figure 1). The white product formed was collected by filtration and washed thoroughly with 100 mL of DMF. The product was characterized by proton nuclear magnetic resonance (¹H NMR) spectroscopy, fluorine NMR (¹⁹F-NMR) spectroscopy, Fourier transform ion cyclotron resonance (FT-ICR) mass spectrometry, N2 and CO2 adsorption, powder X-ray diffraction (PXRD), and scanning electron microscopy (SEM) (Figures S1-S6). Multiple attempts to grow crystals of F-ZrMOC for crystallography characterization were unsuccessful, despite using vapor diffusion, layering, temperature and reaction time variations, different solvents, and varying concentrations of reagents. Purity of synthesis was confirmed via a single peak in 1D NMR (Figures S1 and S2), further evidenced via a single diffusion coefficient in DOSY NMR (Figure 6) and a 3+ produced through ESI-MS (Figure 2), the latter of which appears only when the tetrahedral assembly is present.

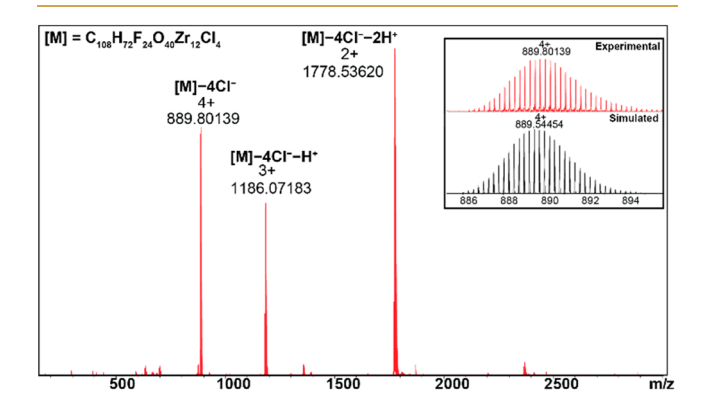


Figure 2. ESI-FT-ICR high resolution mass spectrum of F-ZrMOC in methanol. The inset shows experimental and simulated spectra of the 4+ base peak.

2.3. Computational Details

The starting point geometry was constructed from the crystallographically derived coordinates of the proteo-analog of F-ZrMOC (i.e., ZrMOC formed with terephthalic acid) where the protons were replaced with F atoms at idealized bond lengths.³⁹ The geometry was then optimized and frequency calculation performed using the r²SCAN-3C functional with the def2-mTZVPP basis set.⁴⁰ A CPCM model simulating methanol was used. Both geometry optimization and frequency calculation were performed using

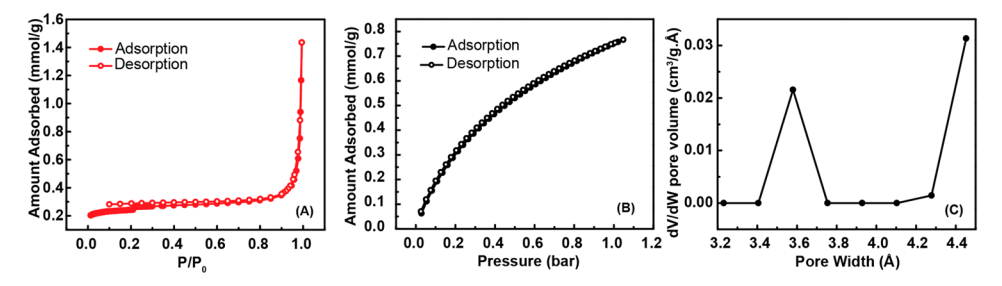


Figure 3. N₂ adsorption isotherm at 77 K (A), CO₂ adsorption isotherm at 273 K (B), and pore size distribution of the F-ZrMOC (C).

ORCA 5.0.3.⁴¹ Several imaginary frequencies were found after the geometry optimization and frequency calculation. However, this is not unexpected, and in some cases unavoidable, for large structures, and visualizing the negative vibrational mode reveals that they corresponded to rotations of the Cp rings. Attempts to reoptimize from several perturbed geometries yield the same results, suggesting that the potential energy surface is relatively flat and possesses many local minima corresponding to slight variations in Cp ring orientation. This is not unexpected and does not detract from any conclusions put forth.

2.4. Sample Preparation and LC-MS/MS Analysis

Solutions were made containing 400 ng/mL of each of the 40 PFAS included in the EPA Draft Method 1633 in 500 μ L of Nanopure water. The F-ZrMOC was added in 10 mg aliquots to the solutions, vortexed, and sonicated for 30 min in 2 mL vials. The sonicated solutions were then transferred to a 1.5 mL Eppendorf tube and centrifuged at 2007g for 10 min. The supernatant was collected and spiked with an isotopically labeled PFAS mixture of 19 compounds at a final concentration of 100 ng/mL (MPFAC-24ES, Table S3) from Wellington Laboratories (Overland Park, KS). Finally, the supernatant was analyzed by LC-MS/MS. This procedure, termed the "standard procedure", was used for all quantification in the experiments below.

The effects of environmental matrix on MOC–PFAS interactions were investigated by using real wastewater and groundwater samples, prepared in triplicate, following the method described in Guardian et al. 42 with minor modifications. Briefly, 500 mL of groundwater and wastewater effluent were adjusted to pH 2.5 \pm 0.5 using glacial acetic acid and loaded onto tandem Oasis HLB and Oasis WAX solid phase extraction cartridges (preconditioned with 10 mL of MeOH and water each) and eluted with 5 mL of 0.1% NH4OH in methanol, methanol, and acetonitrile each at a flow rate of 3–5 mL/min. Eluents were reduced in volume to 500 μ L under a gentle stream of N2 gas at room temperature. The dried extracts were used as matrix samples and spiked to a concentration of 400 ng/mL. The spiked matrix samples were then prepared according to the samples in the procedure in the paragraph above.

2.5. Surface Area and Pore Size Measurements of MOCs Treated with PFAS

Aliquots of activated MOC samples (120.0 mg) were treated with either PFBS or PFOS at a 2:1 mol:mol PFAS:MOC ratio in a 5 mL aqueous solution. After 30 s of vortexing and sonication for 10 min, samples were centrifuged at 2007g for 10 min and the liquid decanted off. The remaining MOC was then rinsed with Nanopure water and activated by evacuating in a vacuum oven at room temperature, until no change in mass was observed. The sample was then transferred to a preweighed tube, further degassed on the Micromeritics VacPrep sample preparation system at 30 °C until no change in mass is observed (~24 h), and surface area and pore distribution analyzed using CO₂ adsorption. Pore size distributions were calculated from the isotherm data using the NLDFT Advanced PSD Method and the model CO₂@273 K on Carbon Slit Pores by NLDFT with a regularization factor of 0.001.

2.6. Cage Capture Optimization

To evaluate the kinetics of PFAS capture by the F-ZrMOC, 2 mg of the MOC was tested in a 500 μ L solution of PFAS (400 ng/mL) at time points ranging from 30 s to 30 min. Samples were prepared for analysis following a standard procedure with the exception of sonication time change between vials. To determine the minimum mass of F-ZrMOC required for optimum PFAS capture, increasing amounts of the cage ranging from 2 to 20 mg were evaluated. Sample preparation followed a standard procedure except for the differing amounts of MOC measured into vials for PFAS capture.

3. RESULTS AND DISCUSSION

3.1. Characterization of the Cage

The F-ZrMOC was synthesized by adopting a method reported in the literature as shown in Figure $1.^{39}$ Characterization of the cage by ¹H NMR revealed that F-ZrMOC possesses protons on the cyclopentadienyl groups (Cp-) and the bridging -OH groups at the metal nodes $(Cp_3Zr_3\mu_3 O(\mu_2(OH)_3)^+$. The singlet at 6.60 ppm corresponds to the protons on the Cp rings (Figure S1). No signal is observed for the -OH group, which can be attributed to deuterium exchange with MeOD; this is supported by the presence of MeOH in the sample spectra. Analysis of the cages by ¹⁹F NMR shows a single peak corresponding to the 24 equiv fluorine atoms on the phenyl rings (Figure S2). Data obtained from FT-ICR mass spectrometry (Figure 2) confirmed the presence of an intact F-ZrMOC with four metal nodes at the vertices bridged by six carboxylate linkers to give a tetrahedral geometry ($[(Cp_3Zr_3\mu_3-O(\mu_2-OH)_3)_4(F_4BDC)_6]^{4+}$), similar to the structure shown in the schematic representation (Figure 1). The mass spectrum (Figure 2) shows peaks at m/z =889.80139, 1186.07183, and 1778.53620 corresponding to $([M]-4Cl^{-})^{4+}$, $([M]-4Cl^{-}+H^{+})^{3+}$, and $([M]-4Cl^{-}+2H^{+})^{2+}$ charged states, respectively.

A nitrogen adsorption isotherm of the cage was collected at 77 K, and a Brunauer-Emett-Teller (BET) area of 20.74 m²/ g was calculated (Figure 3A). The CO₂ adsorption isotherm of the F-ZrMOC was collected at 273 K, and the calculated BET area was 89.56 m²/g (Figure 3B). The aperture size of the proteo-analog of F-ZrMOC with 1,4-benzenedicarboxylate linkers is reported as 3.8 Å, which is close to the kinetic diameter of a N₂ molecule (3.64 Å).³⁹ When CO₂ is used instead of N2, its smaller kinetic diameter (3.30 Å) and the higher temperature at which CO2 adsorption measurements are carried out facilitate to overcome any diffusion limitations and make any ultramicropores (<7 Å) in the sample accessible, resulting in a higher surface area. ⁴³ The pore size distribution from NLDFT calculations demonstrate pore widths of 3.6 and 4.4 Å (Figure 3C), which can be attributed to the intrinsic porosity of the cage and the extrinsic porosity from the cage packing in the solid state, respectively.

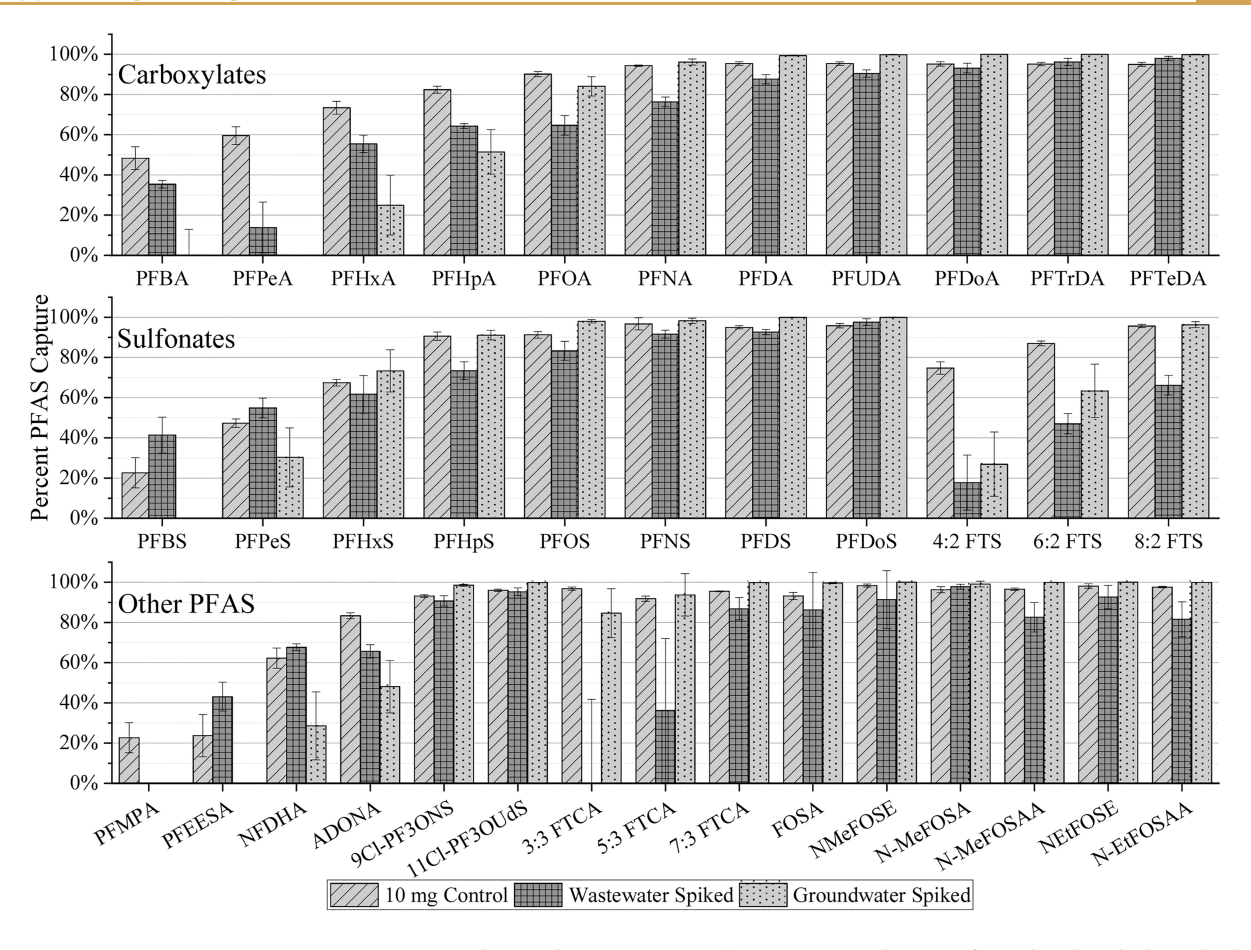


Figure 4. PFAS capture via F-ZrMOC in wastewater and groundwater matrices. The 10 mg control was performed with spiked standards into Nanopure water to exemplify a lack of matrix effects compared with natural water samples. Capture of PFAS of chain lengths seven or shorter is lower in some sulfonic and carboxylic PFAS compared to the control, while capture is maintained for chain lengths eight or greater.

3.2. Wastewater and Groundwater Matrix Tests

An analysis of the "free" PFAS remaining in solution as a function of exposure time during equilibration of F-ZrMOC with the PFAS-containing sample showed immediate capture of PFAS even at the shortest time tested (30 s), suggesting that PFAS interacts with the F-ZrMOC rapidly (Figure S7). We concluded that the adsorption kinetics for PFAS on the F-ZrMOC are fast such that 30 s of equilibration is sufficient to capture PFAS effectively from the aqueous samples. F-ZrMOC was tested in wastewater and groundwater spiked with 40 PFAS at a final concentration of 400 ng/mL using the optimized equilibration time and F-ZrMOC mass to evaluate the impact of matrix on efficiency of PFAS capture. For most PFAS, capture approaches completion in both wastewater and groundwater matrices (Figure 4), especially for species with carbon chain lengths greater than C₇. Despite earlier parameter optimization, capture was ≤50% for PFAS with chain lengths less than C₆. This is most likely due to binding behavior of short chain PFAS: in a study by Loganathan et al., 44 C₄ and C₈ of carboxylic and sulfonic PFAS were modeled for their sorption behaviors. While C₈ PFAS were shown to aggregate in persistent clusters, C₄ PFAS clusters were much less stable, forming and reforming across the experiment. The lower binding can also be partially attributed to the presence of high organic matter that competes with the binding sites in the cage. Similar observations have been reported in MOFs, where a higher amount of the material was necessary to increase % capture of PFAS.²¹ In the referenced work, capture decreased

from near 100% in clean solvent to less than 60%, even when cage amounts were increased more than 2-fold. Certain PFAS were more efficiently captured from wastewater than from groundwater, including PFEESA (43% compared to 4%), NFDHA (68% to 29%), and ADONA (66% to 48%), indicating that ether-containing PFAS are more efficiently captured from the matrix with higher organic matter than groundwater but less than when in the clean control solvent. This suggests the capture capacity of the F-ZrMOC for PFAS chain length C₈ or longer is not limited in matrix-heavy samples and could be a viable PFAS capture material in matrixrich environments. Notably, 3:3 FTCA is not removed in the wastewater spiked matrix. This is most likely due to 3:3 FTCA being a short chain, which is less removed by the F-ZrMOC when subjected to matrix-heavy samples, most likely due to wastewater components that compete with the binding sites. Generally, removal is lower in wastewater samples compared to groundwater samples, indicating that the higher natural organic matter content in wastewater affects the interactions between the PFAS and F-ZrMOC. In addition, removal of shorter chain PFAS is more affected in wastewater than in groundwater, suggesting that the hydrophobic character of PFAS plays a role in the binding with F-ZrMOC. The 3:3 FTCA has much lower hydrophobicity because it is a short chain and contains three carbons that are not fluorinated.

3.3. Flow-Through Simulation

To show that the synthesized F-ZrMOC has practical applications in the rapid filtration of PFAS from contaminated water, cartridges were packed with 20.0 mg of F-ZrMOC and were used as sorbents. PFAS-containing aqueous solutions were passed through these F-ZrMOC-packed cartridges in flow-through experiments and were evaluated in triplicate at two different concentrations. Three cartridges, labeled A1-A3, each had 40 mL of an aqueous PFAS solution containing the 40 PFAS listed in the EPA Draft Method 1633 (8 ng/mL, each) passed through to evaluate capture of a broad range of PFAS. Three cartridges, labeled S1-S3 were evaluated by passing 40 mL of a PFOS solution (50 ng/mL) through to see if breakthrough occurred with an excess of PFAS. Nanopure water was passed through the final three cartridges, labeled M1-M3, for use as a method blank. The average capture rate observed for 20 mg of F-ZrMOC during flow-through experiments was 82% (Figure 5) at PFAS levels well above typical environmental levels.

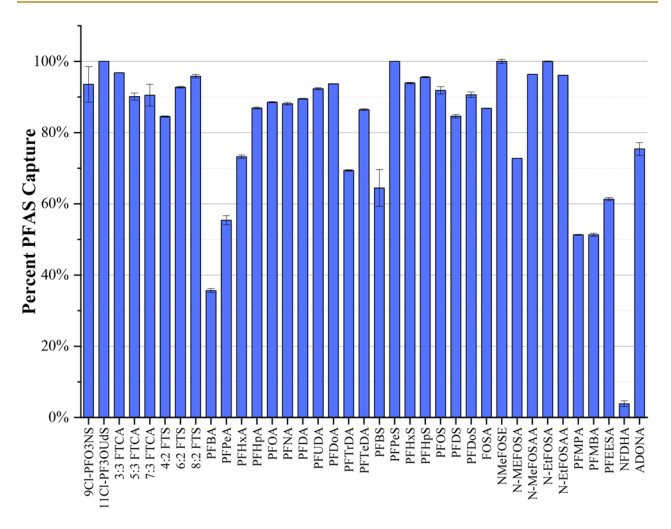


Figure 5. Results of average PFAS capture in A1–A3 with standard deviations using real world simulated flow through. Cartridges were packed with 20 mg of cage to ensure no gaps in the cartridge flow path. Compounds are arranged by class (chlorinated, FTCA, FTS, carboxylic, sulfonic, aminated, ethoxylated) and then by increasing chain length. While ethoxylated and carboxylated PFAS with a chain length shorter than six had decreased capture, PFAS were captured at 80% or above with a low relative standard deviation (1%–3%) with very low exposure time.

3.4. Adsorption Measurements of PFAS-Treated F-ZrMOC

 ${\rm CO_2}$ adsorption measurements of F-ZrMOC samples treated with PFBS and PFOS were performed to identify changes in the pore size distribution and surface area after PFAS treatment that can be indicative of interactions of PFAS with the F-ZrMOC. PFBS and PFOS were chosen to evaluate the effects, if any, of chain length on pore size and surface area. The PFBS-treated MOC sample gave a very slight decrease in surface area ($\sim 84~{\rm m^2/g}$) and an identical pore size distribution (Figure S10) to the pristine F-ZrMOC observed before treatment. It is likely that a majority of PFBS was removed from the F-ZrMOC during the activation process, which requires evacuation of the sample to remove any residual solvents remaining from PFAS treatments prior to measurement. Multiple attempts to measure the ${\rm CO_2}$ adsorption of the

PFOS-treated sample have been unsuccessful due to the inability of the system to achieve equilibrium during the measurement for very long time periods (a single data point was not collected for over a week). We believe this can be caused by PFOS chains blocking the pore apertures of the F-ZrMOC making them inaccessible to CO₂ after PFOS treatment, whereas the shorter chain length of PFBS is presumed to not be able to block the pores. Evidence of residual PFOS even after the BET experiment (attempt) can be seen from the ¹⁹F NMR experiments (Figure S11).

PFBS- and PFOS-treated F-ZrMOC samples were studied by using FTIR-ATR. The normalized spectra show an increase in the peak intensity of the O-H stretching band at ~3200 cm⁻¹ (Figure S12A). This can be attributed to residual water from adsorption experiments. Bridging -OH groups of the Zroxo cluster appear at ~470 cm⁻¹ (highlighted in red, Figure S12B).⁴⁵ There is no significant change in this band for the PFAS-treated cage samples; therefore, we conclude that there is no significant interaction between the cage and PFAS through these bridging OH groups. Peaks corresponding to C-F stretches will usually appear in the 1000-1400 cm⁻¹ region. We can see a growth in the bands at ~1250-1270 cm⁻¹ (highlighted in blue, Figure S12B), as well as new bands growing in the ~1100-1250 region (highlighted in green, Figure S12B) for the PFAS-treated samples. The new peaks in the C-F regions are consistent with the presence of PFAS molecules, but they do not suggest any significant intermolecular attractions that can be monitored by IR. There are also no substantial differences in the other bands outside the C-F range, further indicating that the cage remains intact posttreatment with these two PFAS.

To better understand the solution-state interactions of PFBS with F-ZrMOC, $^{19}\mathrm{F}$ diffusion ordered spectroscopy (DOSY) NMR was performed. A sample of F-ZrMOC treated with PFBS was solubilized in d_4 -methanol, and a two-dimensional $^{19}\mathrm{F}$ DOSY spectrum was acquired. The attenuation of each peak was then fitted, and the results were compiled (Table S2). The 2D DOSY spectrum is illustrated in Figure 6. Two distinct diffusion coefficients are observed, one correlating to resonances assigned to the PFBS moiety $(6.82\times10^{-10}~\mathrm{m}^2/\mathrm{s})$ and the second to F-ZrMOC $(2.12\times10^{-10}~\mathrm{m}^2/\mathrm{s})$.

The observation of different diffusion coefficients suggests that F-ZrMOC and PFBS diffuse separately in a methanol solution. The LC-MS/MS capture experiment data (Figures 4 and 5) provide evidence of decreasing PFAS concentrations in solution with the assumption that they are binding to the F-ZrMOC in aqueous medium; however, these are likely heterogeneous interactions (i.e., dispersed, but not solubilized, F-ZrMOC interacting with aqueous PFAS solutions). We can surmise that the apparent uptake is due to hydrophobichydrophobic interactions between the per- and polyfluoroalkyl chains and the F-ZrMOC cages as a result of C-F groups in both structures.²⁶ When methanol is used as a solvent, the F-ZrMOC solubilizes, disrupting the hydrophobic-hydrophobic interactions and liberating the PFBS, giving rise to the DOSY spectrum acquired. If PFBS chains were encapsulated or otherwise interacting with F-ZrMOC, we would expect to observe correlations of PFBS resonances with a diffusion coefficient corresponding to F-ZrMOC, or larger. The empirically derived diffusion coefficients can be related to hydrodynamic radii using the Stokes-Einstein equation. 46 Converting the radii to diameter gives approximately 11 and 38 Å for PFBS and F-ZrMOC, respectively. These are in good

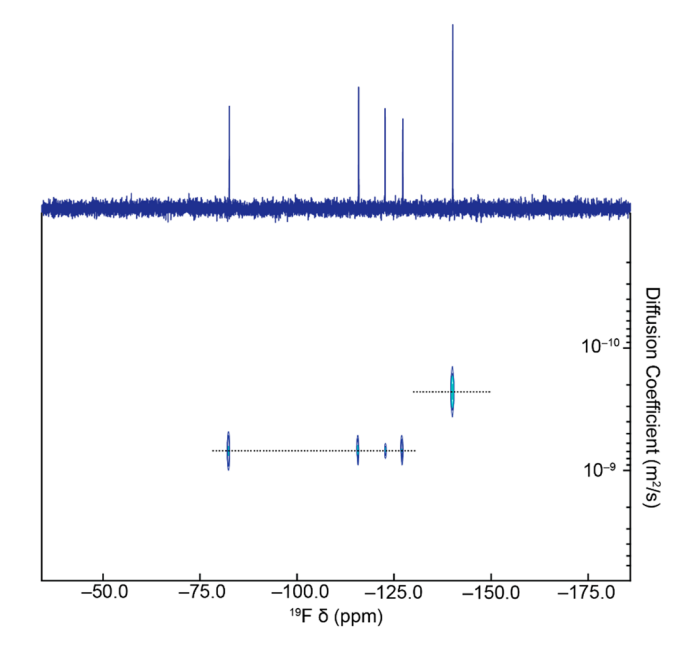


Figure 6. 19F DOSY NMR spectrum of PFBS treated F-ZrMOC. Acquired in d_4 -methanol at 470.4 MHz. Two separate diffusion coefficients suggest that PFBS and the cage diffuse separately.

agreement with the model structures of PFBS (~8 Å) and the optimized structure of F-ZrMOC (21 Å). The small disparities can be accounted for by the addition of a solvation sphere around each species. Additionally, the ¹⁹F NMR and 2D DOSY experiments observe a single peak that is unchanged after adsorption, supporting that the cage remains intact after capture of PFAS.

4. CONCLUSIONS

In this work, we have synthesized a novel fluorinated Zr-based metal-organic cage, F-ZrMOC, to test the hypothesis that its intrinsic porosity and the fluorinated linkers will enhance PFAS-cage intermolecular interactions and thus improve capture performance that can be potentially used for PFAS removal in water. F-ZrMOC exhibits rapid PFAS capture in clean solvent, matrix-heavy samples, and real-world flow through circumstances. The F-ZrMOC is synthesized using a facile synthetic route, allowing for easy scale up. With very short synthesis for large quantities of F-ZrMOC, and very high capture of PFAS across several classes with varying chain lengths, achieved within 30 s, this F-ZrMOC shows great promise as a PFAS remediation tool. While the intrinsic pore size of the cage appears to be too small to trap the PFAS chains completely within the pore, we see from the LC-MS/MS results that the cage captures PFAS molecules from water, likely because of sorption to the surface of the cage. As a next step, we carried out ¹⁹F DOSY experiments and surface area measurements to understand how the cage and the PFAS molecules interact with each other. ¹⁹F DOSY experiments show that the cage and the selected PFAS molecule are independently diffusing in methanol, suggesting that the cage and PFAS molecules interact through hydrophobic-hydrophobic interactions when in water. During surface area and pore size measurements, prohibitively long pressure equilibration times were taken for CO2 adsorption measurements on PFOS-treated F-ZrMOC, implying that the PFAS chains are interacting with the cages in such a way that they block the

apertures of the cage making them inaccessible to CO2; this is supported by ¹⁹F NMR data on the PFOS-treated cage post-BET experiments. Although PFAS capture by the F-ZrMOC was not significantly affected by matrix-heavy samples, short chain and ether-containing PFAS are still more difficult to remove. Future efforts are directed toward the synthesis of cages that can target these PFAS, especially as manufacturers continue to shift toward these alternative, emerging variants.

ASSOCIATED CONTENT

Supporting Information

The Supporting Information is available free of charge at https://pubs.acs.org/doi/10.1021/acsaenm.3c00592.

Methods for analysis and analytical data for the F-ZrMOC: ¹H NMR and ¹⁹F-NMR spectra, FTIR spectra Brunauer-Emmett-Teller plots for N₂ and CO₂ adsorption, powder X-ray diffraction, and scanning electron microscopy; LC-MS/MS parameters for separation and quantification of PFAS; results for quantity and time optimization tests of the F-ZrMOC (PDF)

AUTHOR INFORMATION

Corresponding Authors

Timothy R. Cook - Department of Chemistry, University at Buffalo, The State University of New York, Buffalo, New York 14260, United States; o orcid.org/0000-0002-7668-8089; Email: trcook@buffalo.edu

Diana S. Aga - Department of Chemistry, University at Buffalo, The State University of New York, Buffalo, New York 14260, United States; RENEW Institute, University at Buffalo, The State University of New York, Buffalo, New York 14260, United States; orcid.org/0000-0001-6512-7713; Email: dianaaga@buffalo.edu

Authors

Dino Camdzic - Department of Chemistry, University at Buffalo, The State University of New York, Buffalo, New York 14260, United States; orcid.org/0000-0002-6135-3067

Heshali K. Welgama - Department of Chemistry, University at Buffalo, The State University of New York, Buffalo, New York 14260, United States; o orcid.org/0000-0002-9826-

Matthew R. Crawley – Department of Chemistry, University at Buffalo, The State University of New York, Buffalo, New York 14260, United States; o orcid.org/0000-0002-2555-

Anish Avasthi - Department of Chemistry, University at Buffalo, The State University of New York, Buffalo, New York 14260, United States

Complete contact information is available at: https://pubs.acs.org/10.1021/acsaenm.3c00592

The authors declare no competing financial interest.

ACKNOWLEDGMENTS

The authors acknowledge support from National Science Foundation (NSF) Award# 1905274 to D.S.A. Characterization was carried out using the UBCIC facilities (Bruker SolariXR FT-ICRMS (purchased through NIH S10 RR029517)), and the authors would like to thank Mr. Eric

Jensen for assisting with data collection. NMR experiments were carried out in the UB NMR Center using the Bruker AVANCE NEO 400 and 500 MHz NMR (purchased through NSF CHE-2018160). Adsorption studies were carried out using Micromeritics 3 Flex Surface Area Analyzer (purchased through DOE DEFE0031736 and NSF Award # 1847950 and 2015723). The authors would also like to acknowledge the Materials Characterization Laboratory (MCL) and the Cleanroom at UB for the use of instrumentation. Any opinions, finding, conclusions, or recommendations expressed in this publication are those of the author(s) and do not necessarily reflect the view of the NSF.

REFERENCES

- (1) Occurrence and Use of Highly Fluorinated Substances and Alternatives; KEMI Swedish Chemicals Agency, 2015; pp 361-164.
- (2) PFAS Master List of PFAS Substances; United States Environmental Protection Agency, 2020.
- (3) Akhbarizadeh, R.; Dobaradaran, S.; Schmidt, T. C.; Nabipour, I.; Spitz, J. Worldwide bottled water occurrence of emerging contaminants: A review of the recent scientific literature. *J. Hazard. Mater.* **2020**, 392, 122271.
- (4) Anderson, R. H.; Long, G. C.; Porter, R. C.; Anderson, J. K. Occurrence of select perfluoroalkyl substances at U.S., Air Force aqueous film-forming foam release sites other than fire-training areas: Field-validation of critical fate and transport properties. *Chemosphere* **2016**, 150, 678–685.
- (5) Möller, A.; Ahrens, L.; Surm, R.; Westerveld, J.; Van Der Wielen, F.; Ebinghaus, R.; De Voogt, P. Distribution and sources of polyfluoroalkyl substances (PFAS) in the River Rhine watershed. *Environ. Pollut.* **2010**, *158* (10), 3243–3250.
- (6) Clabby, C. GenX Pollution What Happened? And When?. NC Health News, 2017.
- (7) PFAS; ATSDR, CDC, 2020.
- (8) Joerss, H.; Xie, Z.; Wagner, C. C.; von Appen, W.-J.; Sunderland, E. M.; Ebinghaus, R. Transport of Legacy Perfluoroalkyl Substances and the Replacement Compound HFPO-DA through the Atlantic Gateway to the Arctic Ocean—Is the Arctic a Sink or a Source? *Environ. Sci. Technol.* **2020**, *54* (16), 9958–9967.
- (9) Buck, R. C.; Franklin, J.; Berger, U.; Conder, J. M.; Cousins, I. T.; de Voogt, P.; Jensen, A. A.; Kannan, K.; Mabury, S. A.; van Leeuwen, S. P. Perfluoroalkyl and polyfluoroalkyl substances in the environment: terminology, classification, and origins. *Integr. Environ. Assess. Manag.* **2011**, *7* (4), 513–41.
- (10) Brendel, S.; Fetter, E.; Staude, C.; Vierke, L.; Biegel-Engler, A. Short-chain perfluoroalkyl acids: environmental concerns and a regulatory strategy under REACH. *Environ. Sci. Eur.* **2018**, *30* (1), 9.
- (11) Rice, P. A.; Aungst, J.; Cooper, J.; Bandele, O.; Kabadi, S. V. Comparative analysis of the toxicological databases for 6:2 fluorotelomer alcohol (6:2 FTOH) and perfluorohexanoic acid (PFHxA). Food Chem. Toxicol. 2020, 138, 111210.
- (12) Wallace, J. S.; Edirisinghe, D.; Seyedi, S.; Noteboom, H.; Blate, M.; Balci, D. D.; Abu-Orf, M.; Sharp, R.; Brown, J.; Aga, D. S. Burning questions: Current practices and critical gaps in evaluating removal of per- and polyfluoroalkyl substances (PFAS) during pyrolysis treatments of biosolids. *J. Hazard. Mater. Lett.* 2023, 4, 100079.
- (13) Ateia, M.; Maroli, A.; Tharayil, N.; Karanfil, T. The overlooked short- and ultrashort-chain poly- and perfluorinated substances: A review. *Chemosphere* **2019**, *220*, 866–882.
- (14) Li, F.; Duan, J.; Tian, S.; Ji, H.; Zhu, Y.; Wei, Z.; Zhao, D. Short-chain per- and polyfluoroalkyl substances in aquatic systems: Occurrence, impacts and treatment. *Chem. Eng. J.* **2020**, *380*, 122506.
- (15) Strynar, M.; Dagnino, S.; McMahen, R.; Liang, S.; Lindstrom, A.; Andersen, E.; McMillan, L.; Thurman, M.; Ferrer, I.; Ball, C. Identification of Novel Perfluoroalkyl Ether Carboxylic Acids (PFECAs) and Sulfonic Acids (PFESAs) in Natural Waters Using Accurate Mass Time-of-Flight Mass Spectrometry (TOFMS). *Environ. Sci. Technol.* **2015**, 49 (19), 11622.

- (16) Dickman, R. A.; Aga, D. S. Efficient workflow for suspect screening analysis to characterize novel and legacy per- and polyfluoroalkyl substances (PFAS) in biosolids. *Anal. Bioanal. Chem.* **2022**, *414* (15), 4497–4507.
- (17) Lenka, S. P.; Kah, M.; Padhye, L. P. A review of the occurrence, transformation, and removal of poly- and perfluoroalkyl substances (PFAS) in wastewater treatment plants. *Water Res.* **2021**, *199*, 117187.
- (18) Gebbink, W. A.; van Asseldonk, L.; van Leeuwen, S. P. J. Presence of Emerging Per- and Polyfluoroalkyl Substances (PFASs) in River and Drinking Water near a Fluorochemical Production Plant in the Netherlands. *Environ. Sci. Technol.* **2017**, *51* (19), 11057–11065.
- (19) Herkert, N. J.; Merrill, J.; Peters, C.; Bollinger, D.; Zhang, S.; Hoffman, K.; Ferguson, P. L.; Knappe, D. R. U.; Stapleton, H. M. Assessing the Effectiveness of Point-of-Use Residential Drinking Water Filters for Perfluoroalkyl Substances (PFASs). *Environ. Sci. Technol. Lett.* **2020**, *7* (3), 178–184.
- (20) Huang, J.; Shi, Y.; Xu, J.; Zheng, J.; Zhu, F.; Liu, X.; Ouyang, G. Hollow Covalent Organic Framework with "Shell-Confined" Environment for the Effective Removal of Anionic Per- and Polyfluoroalkyl Substances. *Adv. Funct. Mater.* **2022**, 32 (39), 2203171.
- (21) Li, R.; Alomari, S.; Stanton, R.; Wasson, M. C.; Islamoglu, T.; Farha, O. K.; Holsen, T. M.; Thagard, S. M.; Trivedi, D. J.; Wriedt, M. Efficient Removal of Per- and Polyfluoroalkyl Substances from Water with Zirconium-Based Metal-Organic Frameworks. *Chem. Mater.* **2021**, 33 (9), 3276–3285.
- (22) Li, R.; Alomari, S.; Islamoglu, T.; Farha, O. K.; Fernando, S.; Thagard, S. M.; Holsen, T. M.; Wriedt, M. Systematic Study on the Removal of Per- and Polyfluoroalkyl Substances from Contaminated Groundwater Using Metal-Organic Frameworks. *Environ. Sci. Technol.* **2021**, *55* (22), 15162–15171.
- (23) He, A.; Lu, Y.; Chen, F.; Li, F.; Lv, K.; Cao, H.; Sun, Y.; Liang, Y.; Li, J.; Zhao, L.; Zhang, X.; Li, L.; Wang, Y.; Jiang, G. Exploring the origin of efficient adsorption of poly- and perfluoroalkyl substances in household point-of-use water purifiers: Deep insights from a joint experimental and computational study. *Sci. Total Environ.* **2022**, *831*, 154988.
- (24) Adams, J. Q.; Clark, R. M. Cost Estimates for GAC Treatment Systems. *Journal AWWA* **1989**, *81* (1), 35–42.
- (25) Wang, T. C.; Vermeulen, N. A.; Kim, I. S.; Martinson, A. B. F.; Stoddart, J. F.; Hupp, J. T.; Farha, O. K. Scalable synthesis and post-modification of a mesoporous metal-organic framework called NU-1000. *Nat. Protoc.* **2016**, *11* (1), 149–162.
- (26) Sini, K.; Bourgeois, D.; Idouhar, M.; Carboni, M.; Meyer, D. Metal-organic framework sorbents for the removal of perfluorinated compounds in an aqueous environment. *New J. Chem.* **2018**, 42 (22), 17889–17894.
- (27) Zhang, D.; Ronson, T. K.; Zou, Y.-Q.; Nitschke, J. R. Metalorganic cages for molecular separations. *Nat. Rev. Chem.* **2021**, 5 (3), 168–182.
- (28) Qin, L.-Z.; Xiong, X.-H.; Wang, S.-H.; Meng, L.-L.; Yan, T.-A.; Chen, J.; Zhu, N.-X.; Liu, D.-H.; Wei, Z.-W. A Series of Functionalized Zirconium Metal-Organic Cages for Efficient CO2/N2 Separation. *Inorg. Chem.* **2021**, *60* (23), 17440–17444.
- (29) Chen, S.; Li, K.; Zhao, F.; Zhang, L.; Pan, M.; Fan, Y.-Z.; Guo, J.; Shi, J.; Su, C.-Y. A metal-organic cage incorporating multiple light harvesting and catalytic centres for photochemical hydrogen production. *Nat. Commun.* **2016**, *7* (1), 13169.
- (30) Li, L.; Yang, L.; Li, X.; Wang, J.; Liu, X.; He, C. Supramolecular Catalysis of Acyl Transfer within Zinc Porphyrin-Based Metal-Organic Cages. *Inorg. Chem.* **2021**, *60* (12), 8802–8810.
- (31) Jin, X.; Wang, G.-Q.; Ma, D.; Deng, S.-Q.; Cai, S.-L.; Fan, J.; Zhang, W.-G.; Zheng, S.-R. Cationic Amorphous Metal-Organic Cage-Based Materials for the Removal of Oxo-Anions from Water. ACS Appl. Nano Mater. 2019, 2 (9), 5824–5832.
- (32) Gao, Y.; Deng, S.-Q.; Jin, X.; Cai, S.-L.; Zheng, S.-R.; Zhang, W.-G. The construction of amorphous metal-organic cage-based solid for rapid dye adsorption and time-dependent dye separation from water. *Chem. Eng. J.* **2019**, 357, 129–139.

- (33) Cook, T. R.; Stang, P. J. Recent Developments in the Preparation and Chemistry of Metallacycles and Metallacages via Coordination. *Chem. Rev.* **2015**, *115* (15), 7001–7045.
- (34) Pastore, V. J.; Cook, T. R. Coordination-Driven Self-Assembly in Polymer-Inorganic Hybrid Materials. *Chem. Mater.* **2020**, 32 (9), 3680–3700.
- (35) Pullen, S.; Clever, G. H. Mixed-Ligand Metal-Organic Frameworks and Heteroleptic Coordination Cages as Multifunctional Scaffolds—A Comparison. *Acc. Chem. Res.* **2018**, *51* (12), 3052–3064.
- (36) Fulong, C. R. P.; Guardian, M. G. E.; Aga, D. S.; Cook, T. R. A Self-Assembled Iron(II) Metallacage as a Trap for Per- and Polyfluoroalkyl Substances in Water. *Inorg. Chem.* **2020**, *59*, 6697.
- (37) Liu, G.; Di Yuan, Y.; Wang, J.; Cheng, Y.; Peh, S. B.; Wang, Y.; Qian, Y.; Dong, J.; Yuan, D.; Zhao, D. Process-Tracing Study on the Postassembly Modification of Highly Stable Zirconium Metal-Organic Cages. J. Am. Chem. Soc. 2018, 140 (20), 6231–6234.
- (38) Dalvi, V. H.; Rossky, P. J. Molecular origins of fluorocarbon hydrophobicity. *Proc. Natl. Acad. Sci. U. S. A.* **2010**, *107* (31), 13603–13607.
- (39) Liu, G.; Ju, Z.; Yuan, D.; Hong, M. In Situ Construction of a Coordination Zirconocene Tetrahedron. *Inorg. Chem.* **2013**, *52* (24), 13815–13817.
- (40) Grimme, S.; Hansen, A.; Ehlert, S.; Mewes, J.-M. r2SCAN-3c: A "Swiss army knife" composite electronic-structure method. *J. Chem. Phys.* **2021**, *154* (6), 064103.
- (41) Neese, F.; Wennmohs, F.; Becker, U.; Riplinger, C. The ORCA quantum chemistry program package. *J. Chem. Phys.* **2020**, *152* (22), 224108.
- (42) Guardian, M. G. E.; Boongaling, E. G.; Bernardo-Boongaling, V. R. R.; Gamonchuang, J.; Boontongto, T.; Burakham, R.; Arnnok, P.; Aga, D. S. Prevalence of per- and polyfluoroalkyl substances (PFASs) in drinking and source water from two Asian countries. *Chemosphere* **2020**, 256, 127115.
- (43) Mukhtar, A.; Mellon, N.; Saqib, S.; Lee, S.-P.; Bustam, M. A. Extension of BET theory to CO2 adsorption isotherms for ultramicroporosity of covalent organic polymers. SN Appl. Sci. 2020, 2 (7), 1232.
- (44) Loganathan, N.; Wilson, A. K. Adsorption, Structure, and Dynamics of Short- and Long-Chain PFAS Molecules in Kaolinite: Molecular-Level Insights. *Environ. Sci. Technol.* **2022**, *56* (12), 8043–8052.
- (45) Chavan, S.; Vitillo, J. G.; Gianolio, D.; Zavorotynska, O.; Civalleri, B.; Jakobsen, S.; Nilsen, M. H.; Valenzano, L.; Lamberti, C.; Lillerud, K. P.; Bordiga, S. H 2 storage in isostructural UiO-67 and UiO-66 MOFs. *Phys. Chem. Chem. Phys.* **2012**, *14* (5), 1614–1626.
- (46) Miller, C. C. The Stokes-Einstein law for diffusion in solution. *Proc. R. Soc. London, Ser. A* **1924**, *106* (740), 724–749.